Laser-Driven Compression of Glass Microspheres

P. M. Campbell, G. Charatis, and G. R. Montry
KMS Fusion, Inc., Ann Arbor, Michigan 48106
(Received 4 November 1974)

Volume compressions on the order of 10^2 have been observed in glass microspheres heated by pulses from a Nd glass laser. The degree of compression is inferred from computer analysis of time-integrated x-ray photographs of the target plasma.

The observation of modest neutron yields (10^5–10^6) from laser-driven compression of thermonuclear targets has been reported recently.[1] One of the more important reasons for believing that these experiments have yielded true compression neutrons rather than corona neutrons is the degree of compression indicated in the x-ray photographs of these events. This paper is limited to compression experiments on glass microspheres used as simulated fusion targets. However, the same techniques can also be used to infer compression in targets composed of deuterium or deuterium-tritium.

The laser system used in these experiments consists of a CILAS VK 640 laser with an additional V 80 $A4$ amplifier followed by a Faraday rotator and seven 10-cm clear-aperture GE disk amplifiers. A specially designed ytrium-aluminum-garnet (YAlG) oscillator produces a series of 30-psec (full width at half-maximum) pulses and stacks them together to produce a pulse of the desired temporal form.[2] Various pulses were used in the experiments from exponential to approximately square wave in shape and from 250 to 400 psec in width.

After passing through the GE amplifiers the pulse is split in two and focused on the target by a large-aperture, two-beam optical system which produces a spherically symmetric illumination pattern.[3] The target positioning is accomplished with a system of television cameras and a cw YAlG laser aligned coaxially with the main laser.

Two pinhole cameras are used to take time-integrated photographs of the target in its own x-ray emission. These cameras are oriented 90 deg to each other in a plane perpendicular to the axis of symmetry of the two-beam illumination system. The cameras use 10-μm pinholes and medical no-screen x-ray film which is shielded with an 0.7-mil aluminum absorber. The absorber filters out all of the radiation below about 1.5 keV, giving a (measured) resolution in the target plane of about 14 μm.

Figures 1 and 2 show typical x-ray photographs taken with the experimental arrangement described above. Figure 1 represents a relatively massive shell which did not implode strongly. The ringlike structure occurs just inside the ini-

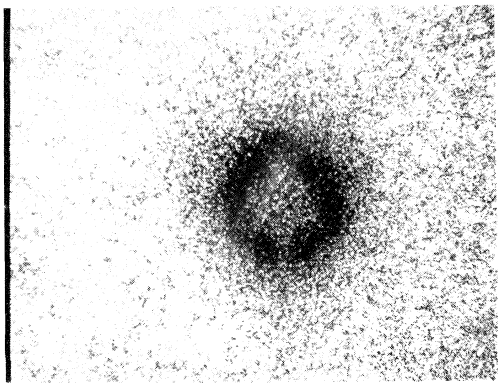

FIG. 1. X-ray pinhole photograph of a 121-μm-diam glass shell with a 2.5-μm wall imploded with a Nd-glass laser. The photograph was taken through a 10-μm pinhole with a magnification of 5 using no-screen medical x-ray film. This photograph shows the ringlike image typical of relatively massive shells which are weakly imploded.

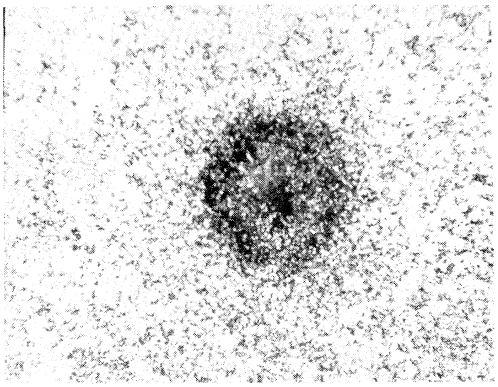

FIG. 2. X-ray pinhole photograph of a 73-μm-diam glass shell with a 1.3-μm wall. The photograph shows the central emission peak associated with more strongly imploded shells.

tial position and is typical of shells which do not acquire a high inward velocity during the time the laser pulse is on. Shells of this type do collapse but not strongly enough for the collapse phase to be visible in the x-ray picture. Figure 2 represents a shell which imploded strongly. Since the shell accelerates from rest, it spends a relatively long time at large radius thereby producing the outer emission ring. After the shell begins to move rapidly inward it does not contribute appreciably to the time-integrated image until the point of maximum compression. At this point the kinetic energy of collapse is converted to thermal energy and a central radiation spike is formed.

Typically the diameter of the central spike is set by the pinhole resolution, and the actual compression achieved cannot be obtained directly from the pinhole photographs. However, considerable information can be obtained by comparing the experimental pinhole forms with those generated from computer simulations of laser-driven implosions. The calculations are capable of matching very accurately the observed pinhole forms and, when such a match is achieved, provide detailed information on the implosion history which could not otherwise be inferred from the data alone.

The basic element in the computer simulation model is a one-dimensional, multifrequency-radiation, hydrodynamics calculation. This calculation is derived from a one-fluid, two-temperature model of the plasma and includes both electron and ion thermal conduction, electron-ion equilibration, ion viscous heating, and radiative transfer.[4] Radiative transfer is handled by means of the variable Eddington approximation[5] and includes bremsstrahlung, recombination, and line mechanisms. Local thermodynamic equilibrium is assumed, since the radiation which forms the x-ray image comes from the dense, inner region of the pellet rather than the hot, low-density corona. Energy levels and partial ionization are calculated using the independent-electron approximation of Mayer.[6,7]

The calculated pinhole form is obtained by post-processing of the temperature and density history given by the implosion calculation. In obtaining the pinhole image the emitted radiation is first passed through the pellet atmosphere where the radiation spectrum is modified by self-absorption. An image is then formed for the pinhole size and camera geometry used in the experiments. This image, which is still multifrequency, is then altered by the aluminum filter and folded into the frequency-dependent film response to give the final pinhole form.

In Fig. 3 the microdensitometer trace of Fig. 1 is shown together with several pinhole forms predicted by the computer simulation code. Since the absorbed energy is not always known with precision experimentally, it is used as a free parameter in the calculations. A nearly exact match to the experimental trace is obtained with the 10-J calculation, which compares favorably with 11 J measured by the blast probe and 12 J measured by the streak camera in this experiment.[8] The maximum density and temperature in the compressed shell as indicated by the calculation were 42 g/cm^3 and 180 eV, respectively.

It should be emphasized that the calculation has matched the actual density distribution on the

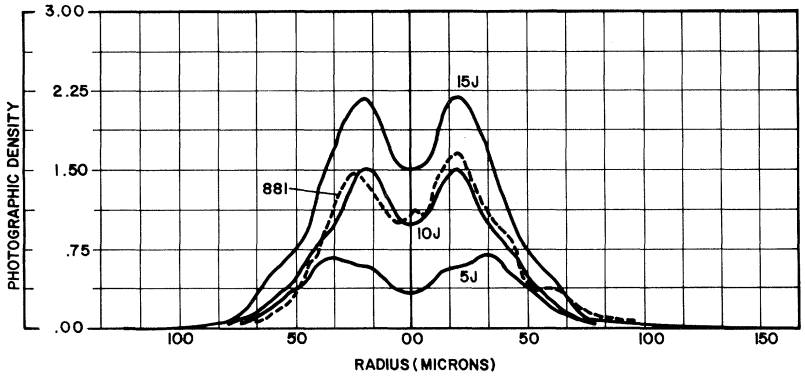

FIG. 3. Comparison of a microdensitometer trace across the image of Fig. 1 (dashed line) with computer predictions for three different values of absorbed energy. The diagram gives the photographic density of the image as a function of radius. The absorbed energy indicated by the calculation is very close to the values determined experimentally: 11 J from the blast probe and 12 J from the streak camera.

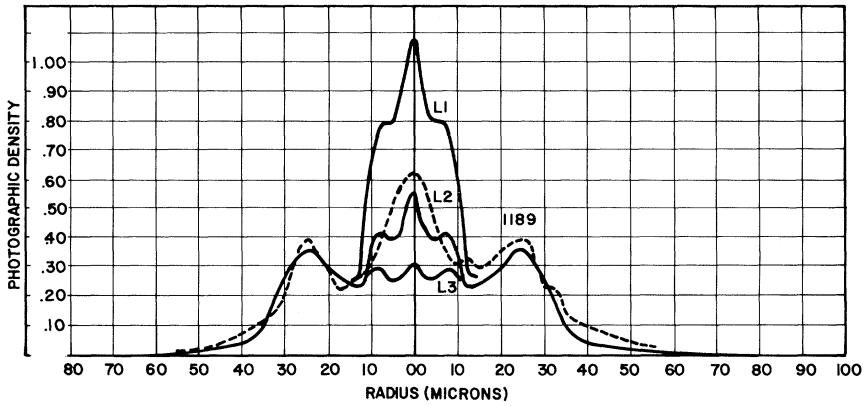

FIG. 4. Comparison of the microdensitometer trace of Fig. 2 (dashed line) with computer predictions for different degrees of central convergence resulting from illumination asymmetry. In the three cases shown the inner wall of the shell penetrated to 4.5, 5.2, and 5.7 μm, respectively. The absorbed energy required for the computer match was 3.3 J which compares closely with 4 J in the slow-ion component measured experimentally.

film and not just the relative form of the image. In this sense it is an independent measure of the x-ray dose in the range of 1 to 4 keV.

In Fig. 4 the computer match to the microdensitometer trace of Fig. 2 is shown. In strongly imploded shells, the calculated position of the outer ring is primarily determined by the shell thickness and absorbed energy, whereas the central maximum is determined by the absorbed energy and the degree of spherical convergence. When the amount of absorbed energy is found which gives the outer ring correctly, the central convergence usually has to be limited in order to match the height of the central maximum. This gives a good indication of the extent to which symmetry was degraded in the experiment.

Two-dimensional computer runs indicate that when the spherical convergence is only slightly degraded by illumination asymmetry the effect is equivalent to the addition of a small amount of tangential velocity to the otherwise radially converging material. This effect can, therefore, be included in a one-dimensional calculation by the addition of a small amount of angular momentum to the material initially. The infinitesimal elements which compose the spherical shell are assumed to have their angular momentum vectors oriented uniformly so that the shell always moves spherically but is limited in its minimum distance of approach to the center.

In Fig. 4 the experimental trace is compared with calculated traces for three different angular momentum values L_1, L_2, and L_3 corresponding to initial tangential velocities of 2.0×10^6, 2.2×10^6, and 2.5×10^6 cm/sec, respectively. In these calculations the inner wall of the shell penetrated to 4.5, 5.2, and 5.7 μm, respectively, which gives a good idea of the degree of spherical convergence achieved in the experiment. Since the initial radius of the inner wall was 35.2 μm, the best computer match indicates a volume compression of 330.

All three of the calculated pinhole forms required an absorbed energy of 3.3 J in order to match the position of the outer ring. The absorbed energy measured experimentally by charge cups was 4 J in slow ions and 2 J in fast ions.[3] It is believed that the fast ions are electrostatically accelerated in the corona, and that they have only a weak effect on the implosion. One finds, generally, that the absorbed energy derived from the pinhole match compares closely with the slow-ion component measured by the charge cups.

In general, pinhole traces of the form shown in Fig. 2 require a two-parameter fit based on absorbed energy and the degree of convergence. Experience has shown that the amount of absorbed energy required for the fit usually agrees very closely with measured values. Usually there is no independent check on the degree of convergence.

It is a pleasure to acknowledge valuable contributions in almost all phases of this work by Dr. K. A. Brueckner.

[1]R. R. Johnson, Bull. Amer. Phys. Soc. 19, 886(A)

(1974).
[2]C. E. Thomas and L. Siebert, "Laser Pulse Stacker" (to be published).
[3]C. E. Thomas, "Laser Fusion Illumination System" (to be published).
[4]L. Spitzer, *Physics of Fully Ionized Gases* (Interscience, New York, 1962).
[5]G. C. Pomraning, *The Equations of Radiation Hydrodynamics* (Pergamon, New York, 1973), p. 51.
[6]H. Mayer, LASL Report No. LA-647, 1947 (unpublished).
[7]B. Kivel and H. Mayer, J. Quant. Spectrosc. Radiat. Transfer 5, 13 (1965).
[8]T. Leonard and F. Mayer, private communication.

Normal Modes in the Ion-Beam–Plasma System

D. Grésillon and F. Doveil
Laboratoire de Physique des Milieux Ionisés, Ecole Polytechnique, 75230 Paris 5e, France*
(Received 24 June 1974)

Two types of dispersion relations are experimentally shown to exist in an ion-beam–plasma system. For beam velocities close to the ion-sound speed, two normal modes, one unstable, are seen. For larger beam velocities, the interferometer output exhibits beating between the three predicted stable normal modes, which are the "fast" and "slow" ion-beam modes and the plasma ion-acoustic wave.

The effects of an ion beam injected into a plasma have received an increasing interest in the recent years. Domains for instabilities have been predicted by linear kinetic theory,[1] whereas experiments have mainly been done on nonlinear effects. The occurrence of beam-generated noise has been observed, and the diffusion of ions in velocity space was reported in magnetized[2] and unmagnetized[3,4] plasmas. The parametric decay of a beam mode,[5] stationary waves in cylindrical geometry,[6] and large-amplitude waves[7,8] have also been observed. All of these nonlinear effects depend on extensions of linear normal-mode theory. However, except for time-of-flight experiments[3,4] observations of the linear dispersion relation in the ion-beam–plasma system have not yet been reported. We thus wish first to state the predictions of linear theory, and then to evidence the experimental existence of such predicted, simultaneous modes.

When an ion beam of density n_b, with a drifting Maxwellian distribution (mean velocity v_b and temperature T_b), is introduced into a plasma with stationary ions (density n_p, temperature T_p) and electrons ($n_e = n_b + n_p$, T_e), the kinetic dispersion relation[1] can be written

$$1 - K^{-2} \int dV\, (V - W)^{-1}\, \partial F/\partial V = 0. \qquad (1)$$

Equation (1) relates the wave phase velocity to the wave number K. The normalizing factors are the ion-sound speed $c_s = (T_e/m_i)^{1/2}$ for the phase velocity $W = \omega/kc_s$, and the Debye length $\lambda_D = (\epsilon_0 T_e/n_e e^2)^{1/2}$ for the wave number $K = k\lambda_D$. $F(V)$ is the total distribution function, comprised of plasma ions, beam ions, and electrons. In consistent units, it is written

$$F(V) = (2\pi)^{-1/2}\{(1-\alpha)\theta^{1/2}\exp(-\theta V^2/2) + \alpha\theta_b^{1/2}\exp[-\theta_b(V-V_b)^2/2] + R^{1/2}\exp(-RV^2/2)\},$$

where $\alpha = n_b/n_e$ is the ion-beam relative density, $\theta = T_e/T_p$ is the plasma-ion temperature ratio, $\theta_b = T_e/T_b$ is the beam-ion temperature ratio, $V_b = v_b/c_s$ is the beam mean velocity, and $R = m_e/m_i$ is the mass ratio.

In the long-wavelength limit, and in the absence of a beam ($\alpha = 0$), the principal root of Eq. (1) is the stable plasma ion-acoustic mode, with phase velocity close to 1 (or -1). In the absence of ions at rest ($\alpha = 1$), these two ion-acoustic solutions are simply Doppler shifted, to a fast ion-beam mode (velocity $V_b + 1$) and a slow ion-beam mode (velocity $V_b - 1$). All these modes are still expected to exist for intermediate values of α, and provide the starting points for iteratively solving Eq. (1).

The real part of the phase velocity of these principal modes is shown in Fig. 1, as a function of beam velocity. The full lines are the theoretical results for $\alpha = 0.1$ and equal temperature ratios $\theta = \theta_b = 20$ (all velocities normalized to c_s).

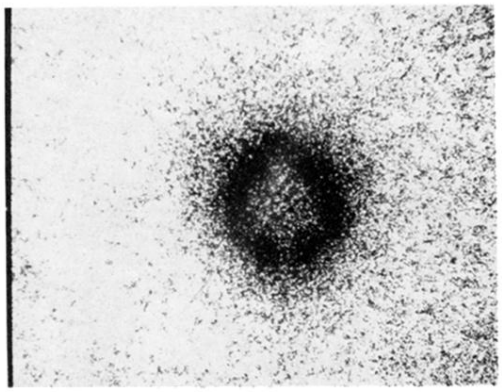

FIG. 1. X-ray pinhole photograph of a 121-μm-diam glass shell with a 2.5-μm wall imploded with a Nd-glass laser. The photograph was taken through a 10-μm pinhole with a magnification of 5 using no-screen medical x-ray film. This photograph shows the ring-like image typical of relatively massive shells which are weakly imploded.

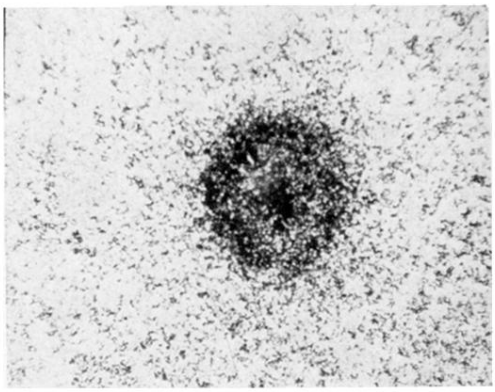

FIG. 2. X-ray pinhole photograph of a 73-μm-diam glass shell with a 1.3-μm wall. The photograph shows the central emission peak associated with more strongly imploded shells.